Kasetsart J. (Nat. Sci.) 49 : 1012 - 1021 (2015)

On the Parallel Simulation of Microparticle Capture in Axial Magnetic Filter

Kanok Hournkumnuard[1], Witchaya Pornjarungsak[2] and Chantana Chantrapornchai[3,*]

ABSTRACT

A parallel algorithm was developed to simulate the capture of weakly magnetic microparticles by parallel ferromagnetic wires randomly distributed in an axial magnetic filter. The problem of microparticle capture was considered within a representative cylindrical cell composed of a representative wire and a surrounding fluid medium. The radius of the cell relative to the wire was determined by the volume fraction of the wires contained within the filter. The magnetic and axial fluid flow fields around the representative wire were determined by the effective medium and the multi-wire models, respectively. All possible trajectories within a representative cell were calculated and analyzed to evaluate the filter efficiency. The number of trajectories was quite large and it took more than 1 hr to obtain the filter efficiency for a set of operating parameters. To speed up the simulation, the work was implemented using parallel programming based on OpenMP. The accuracy of the results was verified against the sequential version. The simulation system was composed of three modules: the user interface module which obtains the operating parameters from the user, the computing module and the graphical display module. The maximum gain was 5.27 times faster and the predicted capture areas and capture efficiencies from the sequential and parallel programming agreed with each other.

Keywords: microparticle capture, parallel simulation, OpenMP, axial magnetic filter

INTRODUCTION

For many years, a high gradient magnetic field has been applied in biomedical applications for trapping biological entities from suspensions such as normal and infected blood cells, other biological cells and immunoglobulin (Melville *et al*., 1975; Han *et al.,* 2006; Inglis *et al*., 2006; Jung *et al*., 2008; Ribaut *et al*., 2008; Hackett *et al*., 2009; Hiroshi *et al*., 2009; Bhakdi *et al*., 2010; Philipp *et al*., 2012) or for determining the magnetic properties of biological particles (Norina *et al*., 2014). Moreover, a high gradient magnetic field is also used in environmental applications for separating phosphate from inland water (Martos *et al*., 2011). The advantage of a high gradient magnetic field is that it provides a magnetic force which is strong enough to capture even biological or environmental entities which have weakly magnetic properties (para- or diamagnetism). The capture of microparticles using magnetic means has several advantages as the particles are

1 Department of Physics, Faculty of Science, Silpakorn University, Nakhon Pathom 73000, Thailand.

2 Departmentof Computing, Faculty of Science, Silpakorn University, Nakhon Pathom 73000, Thailand.

3 Department of Computer Engineering, Faculty of Engineering, Kasetsart University, Bangkok 10900, Thailand.

* Corresponding author, e-mail: fengcnc@ku.ac.th

Received date : 26/04/15 Accepted date : 14/12/15

separated via their differences in intrinsic magnetic properties and the separation process requires minimal adjustment of their chemical properties. Magnetic filters consist of ferromagnetic wires which play the role as the capture center as shown in Figure 1.

The former work of Hournkumnuard and Natenapit (2013) sequentially simulated the capture of red and white blood cells by an axial magnetic filter containing randomly distributed parallel ferromagnetic wires. The current work modified their simulation algorithm into a parallel version and developed a graphical representation module.

BACKGROUND

The theoretical background of the sequential simulation by Hournkumnuard and Natenapit (2013) consists of three main parts. The first part is the concept of the representative cell. By noting that an arbitrary wire is surrounded by other randomly distributed wires, all wires are under the same conditions of magnetic and fluid flow fields. Then the system of wires and surrounding fluid medium within the filter composed of many identical cells is modeled. Each cell contains only one wire surrounded by the fluid medium. The relative size between the wire and the cell is determined by the volume fraction of the wires within the filter. Then, filter operation can be simulated by operation of only a representative cell while all other cells are treated as an effective medium. Figure 2 shows a representative cell in the effective medium with associated Cartesian axes and cylindrical coordinates (r, θ, z).

Figure 1 Ferromagnetic wires as capture centers in magnetic filter.

In Figure 2, the wire of radius a is contained within the cell of radius b. The ratio a^2/b^2 is equal to the volume fraction of the wires contained within the filter (denoted by γ). The z axis of the coordinate system is parallel to the wire axis. The second part is the modeling of the magnetic field around the representative wire. The result of Natenapit and Sanglek (1999) was adapted as shown in Equation 1:

$$\vec{H} = A\vec{H}_0\left[\left(1+\frac{K_C}{r_a^2}\right)\cos\theta\ \hat{r} - \left(1-\frac{K_C}{r_a^2}\right)\sin\theta\ \hat{\theta}\right], \quad 1 \le r_a \le b/a \tag{1}$$

where $r_a = r/a$ is the normalized radial distance, $A = 1/(1-\gamma K_C)$, $K_C = (\nu-1)/(\nu+1)$, $\nu = \mu_C/\mu_f$, μ_C and μ_f are the magnetic permeability of the wire and the surrounding fluid medium, respectively. The field $\vec{H}_{eff}$ within the effective medium is shown in Equation 2 (Natenapit and Sanglek, 1999):

$$\vec{H}_{eff} = \vec{H}_0, \ r_a > b/a. \tag{2}$$

The magnetic field within the effective medium has no gradient. The particles that escape the cell into the effective medium are not subjected to the magnetic force and are transported by the fluid flow.

The third part is to model the fluid flow fields around the representative wire by using the expression of the viscous laminar flow field parallel to an assemblage of randomly distributed cylinders reported in the work of Happel (1959) as shown in Equation 3:

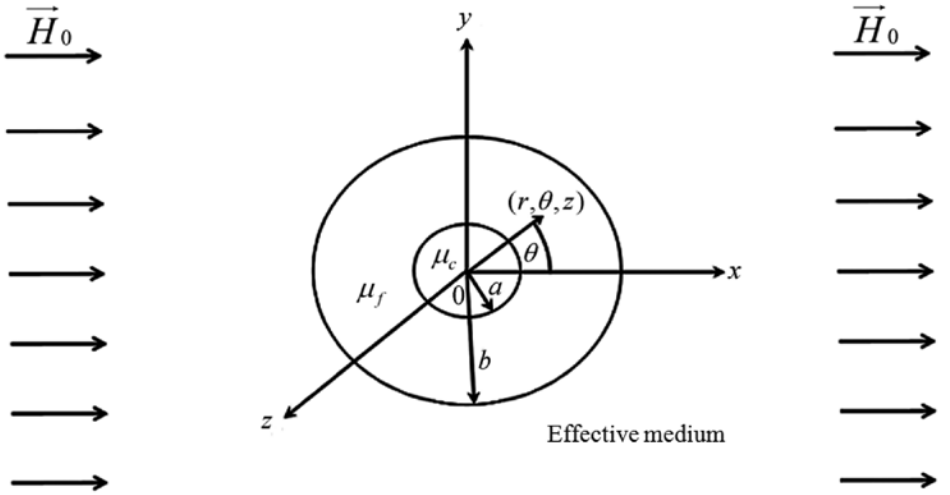

Figure 2 Representative cell in the effective medium with associated coordinates (r, θ, z), where θ is the angle, a is the wire radius, b is the cell radius, μ_C and μ_f are the magnetic permeability of the wire and the surrounding fluid medium, respectively, 0 is the origin of coordinate system and $\vec{H}_0$ is the uniform magnetic field from an external source.

$$\vec{v}_f(r_a) = \frac{\gamma(V_0/a)}{2Ku}(1 - r_a^2 + \frac{2}{\gamma}\ln r_a)\hat{z}, \quad 1 \le r_a \le b/a \tag{3}$$

where V_0 is the speed of the fluid when it enters the filter, $Ku = \gamma - 0.5\ln\gamma - 0.25\gamma^2 - 0.75$ is the Kuwabara factor. The fluid velocity within the effective medium is constant and equal to V_0 as shown in Equation 4 (Happel, 1959):

$$\vec{v}_f = V_0\hat{z}, \quad r_a > b/a. \tag{4}$$

Then, the equation of motion of arbitrary particle within the cell is formulated, taking into account the influence of magnetic and fluid drag force, as shown in Equation 5:

$$m_p \frac{d\vec{v}_p}{dt} = \vec{F}_m - 6\pi\eta_f b_p(\vec{v}_p - \vec{v}_f). \tag{5}$$

The exact solution of Equation 5 can be obtained as Equation 6:

$$\vec{v}_p(t) = (\vec{v}_f + \frac{\vec{F}_m}{6\pi\eta_f b_p}) + (\vec{v}_{p0} - \vec{v}_f - \frac{\vec{F}_m}{6\pi\eta_f b_p}) e^{-(\frac{6\pi\eta_f b_p}{m_p})t} \tag{6}$$

where $\vec{v}_{p0}$ is local particle initial velocity at a position, η_f is the fluid viscosity, b_p is particle radius. For a microparticle, the factor $6\pi\eta_f b_p / m_p$ is in the order of 1×10^{-10} s^{-1} so, at any instance of time, the particle velocity at a position within the cell can be approximated as Equation 7:

$$\vec{v}_p(r_a) = \vec{v}_f(r_a) + \frac{\vec{F}_m(r_a)}{6\pi\eta_f b_p}. \tag{7}$$

In Equation 7, the magnetic force can be determined as in Equation 8 (Hournkumnuard and Natenapit, 2013):

$$\vec{F}_m = \mu_0(\chi_p - \chi_f)V_p H\vec{\nabla}H \tag{8}$$

where V_p is the volume of a particle, χ_p and χ_f are the magnetic susceptibility of the particle and fluid, respectively. Substituting Equation 1 into Equation 8, the explicit expression of magnetic force is obtained as shown in Equation 9:

$$\vec{F}_m = -f_{m0}\left[\left(\frac{\cos 2\theta}{r_a^3} + \frac{K_C}{r_a^5}\right)\hat{r} + \left(\frac{\sin 2\theta}{r_a^3}\right)\hat{\theta}\right] \tag{9}$$

where

$$f_{m0} = \frac{4\pi\mu_0(\chi_p - \chi_f)K_C A^2 H_0 b_p^3}{3a}.$$

The components of the magnetic force exists only on the plane perpendicular to the wire axis (z axis). The particle motion in the z direction is governed by the fluid flow field. From Equation 7, the system of coupled ordinary differential equations for coordinates (r_a, θ, z_a) can be expressed in Equations 10a–10c (Hournkumnuard and Natenapit, 2013):

$$\frac{dr_a}{dt} = -V_{ma}A^2\left(\frac{K_C}{r_a^5} + \frac{\cos 2\theta}{r_a^3}\right), \quad (10a)$$

$$\frac{d\theta}{dt} = -V_{ma}A^2\left(\frac{\sin 2\theta}{r_a^4}\right), \quad (10b)$$

$$\frac{dz_a}{dt} = \frac{\gamma(V_0/a)}{2Ku}\left(1 - r_a^2 + \frac{2}{\gamma}\ln r_a\right) \quad (10c)$$

where $V_{ma} = 4\mu_0(\chi_p - \chi_f)H_0^2 b_p^2 K_c / 9\eta a$ is the magnetic velocity and $z_a = z/a$ is the axial distance in the unit of wire radius.

To obtain particle trajectories, all possible initial coordinates (r_{a0}, θ_0, z_{a0}) are assigned and then Equations 10a–10c are solved, using the standard 4th-order Runge-Kutta method, to obtain new coordinates (r_a, θ, z_a) at later time steps for particle trajectories. The calculation of new coordinates (r_a, θ, z_a) continues until the particle touches the wire surface ($r_a \leq 1 + (b_p / a)$) or escapes the cell. Once a trajectory starting from the initial coordinates is obtained, the last status of the particle is examined to determine whether it is captured by or escapes the filter. Then, for each angle θ, the maximal r_{a0} of initial coordinates that cause the particle to be captured are determined and this is called maximal r_{a0} as "the capture radius, R_C" for the angle θ. Once the capture radius for every angle θ has been obtained, a curve is traced which connects every R_C together and the area between the wire surface and the curve is called "the capture area, A_C". Finally, the filter efficiency (ε) can be determined from the relation in Equation 11 (Hournkumnuard and Natenapit, 2013):

$$\varepsilon = \frac{\gamma A_C}{\pi a^2}. \quad (11)$$

Figure 3 demonstrate an example of the capture radius (R_C) and capture are (A_C) for the condition of $\chi_p - \chi_f > 0$.

For the practical operating parameters of an axial filter, the number of possible trajectories is quite large (within the order of 1×10^5 to 1×10^6 trajectories). Furthermore, the time step used in the 4th-order Runge-Kutta method should be small enough to ensure computational stability. According to these factors, determining the filter efficiency for a set of operating parameter requires a time interval of more than 1 hr and a parallel algorithm is necessary to obtain accurate simulation results within a reasonable time. Hournkumnuard and Natenapit (2013) studied the efficiency of capturing red and white blood cells from a blood sample using an axial magnetic filter.

Parallel simulation of microparticle capture in a magnetic filter working in transverse and longitudinal modes was developed by Chantrapornchai *et al*. (2012). In their work, the particle trajectories on a plane perpendicular to the wire axis were calculated and analyzed in parallel using OpenMP. Then, all trajectories were plotted using OpenCV and finally the filter efficiency was reported. The number of trajectories to be calculated and plotted is in the order of 1×10^2 and the total time of the parallel simulation is rather short. The simulation in the current work is rather complex because particles travel in three dimensional space and the number of trajectories is quite large.

MATERIALS AND METHODS

Parallel simulation was designed where each thread was computed independently based on an angle interval. Because of the symmetry

of the magnetic force, which can be seen easily from Equation 9, and the axial symmetry of fluid velocity, the capture can be considered only within one quadrant on the plane perpendicular to the wire axis as shown in Figure 4. The range of the angle is 0–90°. The granularity of the angle can be divided into 0.5° amounts. The master thread computes at 0° and the slave threads compute the

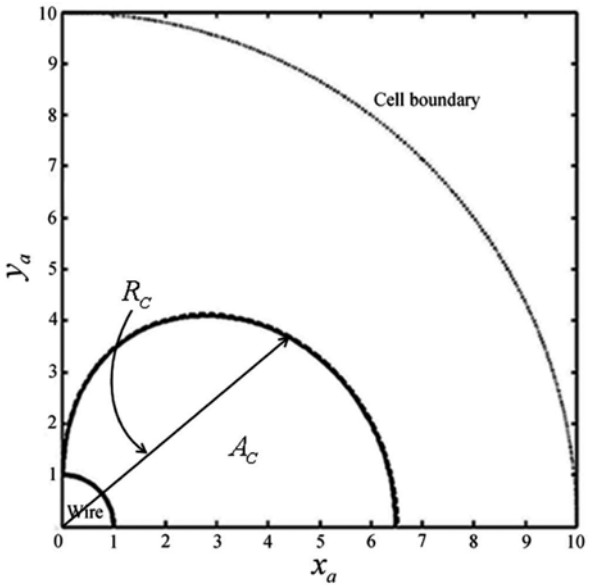

Figure 3 Example of capture radius (R_C) and capture area (A_C) for the condition of $\chi_p - \chi_f > 0$, where the horizontal (x_a) and vertical (y_a) axes are coordinates on a plane perpendicular to the wire, measured in units of wire radius (a).

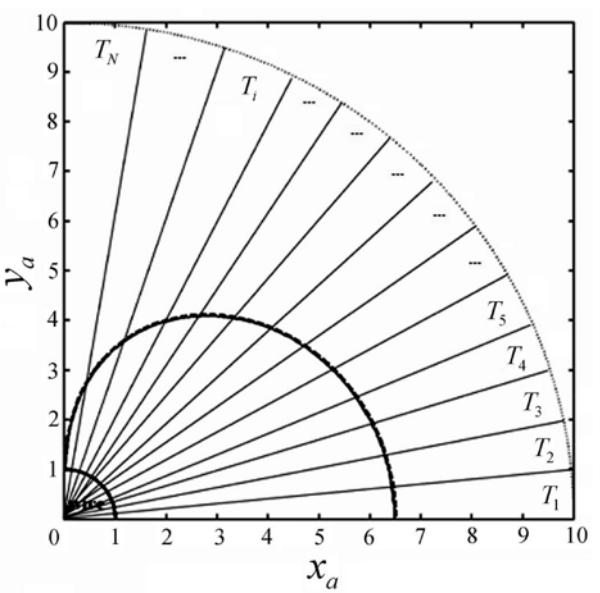

Figure 4 The distribution of simulation domain in a representative cell to various threads, where horizontal (x_a) and vertical (y_a) axes are coordinates on a plane perpendicular to the wire axis, measured in units of wire radius (a) and T_1, T_2, T_3, T_4, T_5, …, T_i, …, T_N are thread labels.

results for the angle they are assigned and return the results to the master thread. Then the master thread uses the collected results to display the capture radii and capture area and to calculate the capture efficiency.

The algorithm for determining the capture radius for each angle θ can be described as follows.

Step 1: Compute the trajectory from various initial positions of angle θ as follows.

1.1 Picking up the old coordinates $(r_a, \theta, z_a)_i$ at present time step t_i. (At initial time t_0, = 0, the old coordinates are the start position $(r_{a0}, \theta_0, z_{a0} = 0)$).

1.2 Obtain new coordinates $(r_a, \theta, z)_{i+1}$ at next time step $t_{i+1} = t_i + \Delta t$ by solving the system of the differential Equations 10a–10c using the 4th-order Runge-Kutta method.

1.3 Check status of new coordinates $(r_a, \theta, z)_{i+1}$ as follows

Case 1: if $((r_a)_{i+1} \leq 1.0 + (b_p / a))$ and $((z_a)_{i+1} < (\textit{filter length} / a))$ then record that the particle starting from present initial coordinates is captured on the wire and finish trajectory computing.

Case 2: if $((z_a)_{i+1} \geq (\textit{filter length} / a))$ then record that the particle starting from the present initial coordinates escapes the filter and finish trajectory computing.

Case 3: if $((r_a)_{i+1} > 1.0 + (b_p / a))$ and $((z_a)_{i+1} < (\textit{filter length} / a))$ and $((r_a)_{i+1} < \textit{cell\_radius} / a))$ then the particle is not captured but still travels within the cell so jump to Step 1.1 through 1.2 until the condition in case 1 or 2 is true.

Step 2: Determine and record for each angle θ the capture radius R_C which is the maximal initial r_{a0} for the capture of that particle starting from this position.

The capture radius for every angle θ is determined in parallel. Once the capture radius for every angle θ has been obtained, the capture area can be obtained from the master thread by numerically integrating the area between the wire surface and the curve that connects the capture radius of every angle together. Figure 5 shows how to divide the work for each thread.

Various thread schedules were studied in OpenMP in the simulation: static, dynamic and guided dynamic. The static method divides the number of works per thread at compile time and the dynamic method assigns the work to the thread when the thread finishes the current work execution. The work size is given as a constant parameter, known as the chunk size. For a guided-dynamic schedule, the remaining work size is calculated during the run time to assign to the available threads.

The user interface window was designed for the simulation as shown in Figure 6. There are two menus for the user; the menu "File" for saving present operating parameters or recalling previously saved parameters; and the menu "Clear" for resetting all parameters. The type of

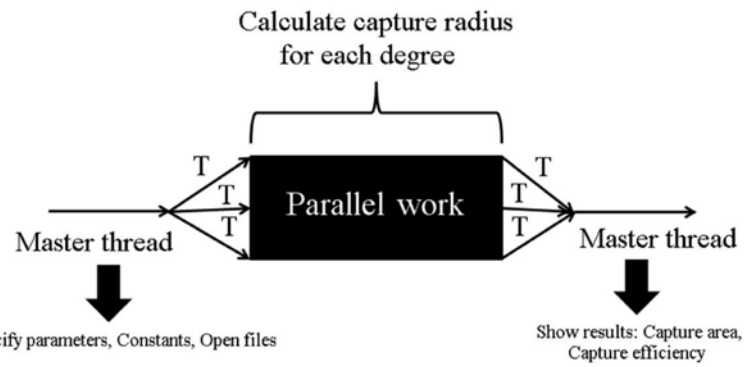

Figure 5 Parallelization of computing work for determining capture radius for each angle.

OpenMP schedule is indicated on the upper left position of the window. The parameter name (in Thai language and script), the parameter setting tool and the unit of the parameter are under the schedule type. Some parameters are set by selecting a value within the assigned range. Some parameters are set using a sliding bar.

The following simulation parameters and their ranges were assigned: 1) the strength of the uniform magnetic flux density ($\vec{B}_0 = \mu_0 \vec{H}_0$) from the external source within the range 0.1 to 0.5 Tesla (T); 2) the speed of fluid flow when it enters the filter (V_0) in the unit within the range 0.01 to 0.10 m.s^{-1}; the average radius of the target particle (b_p) within the range 1×10^{-4} to 1×10^{-6} m; 3) the average radius of the wire (a) within the range 1×10^{-4} to 2×10^{-4} m; 4) volume packing faction of the wires in the filter (γ) within the range 0.01 to 0.07; the length of the filter (l) within the range 0.10 to 0.30 m; 5) the time step used in the 4th-order Runge-Kutta method (Δt) within the range 1×10^{-6} to 1×10^{-5} s; the number of threads (num_thread) assigned by selecting an integer from 2, 4, 8 or 16 threads; 6) the chunk size value as an integer with a value from 1 to 80 specifying the work for each thread.

RESULTS AND DISCUSSION

Figure 7 shows the simulation time for each schedule in OpenMP for various cases of thread number. Assumptions made were: work size = 1, and N_job for the static case. N_job is the total_work per num_thread where the total_work is the number of angles of θ for calculating the capture radius. For the dynamic case, it was assumed work size = 1 and N_job. The test processor was an Intel Xeon 2.93GHz 4 cores per 8 threads with 16G RAM. The performance was about the same, with the static schedule with chunk size=1 yielding the best performance. The execution time of each schedule type is shown in Figure 7, where the speed gain obtained was up to 5.27 times for 16 threads in Figure 8. Note the sequential version took 4,351.25 s on the same machine and it took 824 s using 16 threads in the parallel version.

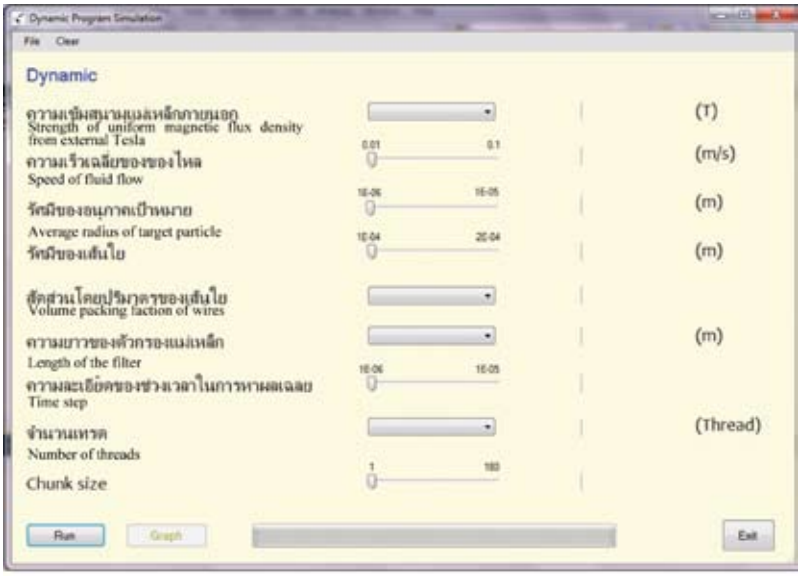

Figure 6 Components of user interface window with a superimposed English translation for clarification in the figure.

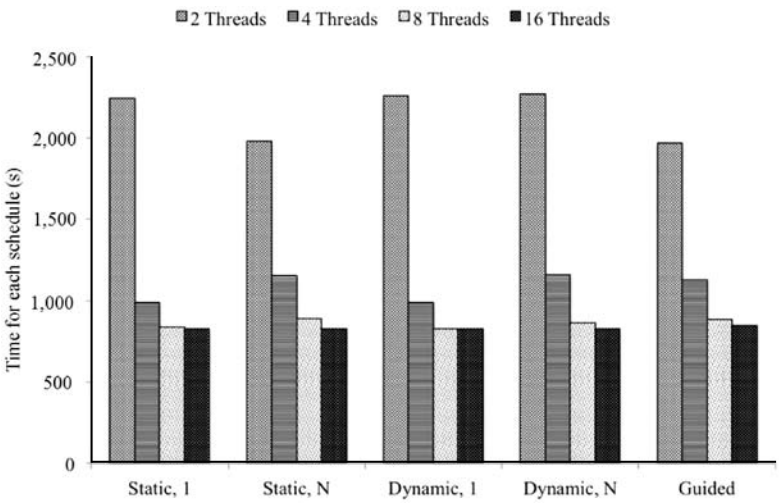

Figure 7 Simulation time for each schedule in OpenMP for various cases of thread number.

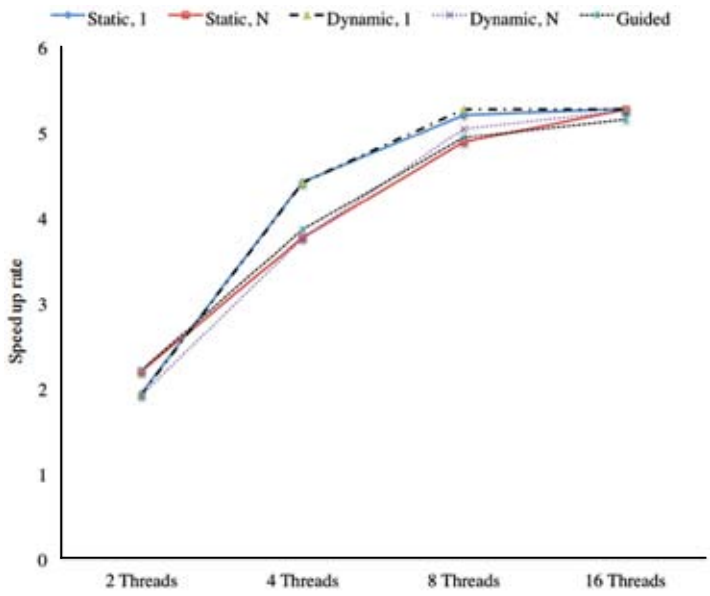

Figure 8 Speed up rate of various schedules.

Figure 9 shows the result window displaying the cell boundary, the capture area and the extent of the wire surface, assigned simulation parameters and the predicted filter efficiency.

The parameters that provide the result in Figure 8 are B_0 = 0.1 T, V_0 = 0.01 m.s^{-1}, b_p = 1.0 μm, a = 100.0 μm, γ = 0.05, l = 0.10 m and $\triangle$t = 1.0 × 10^{-5} s. The predicted filter efficiency of 34.99 % obtained from parallel simulation was compared to the original work of Hournkumnuard and Natenapit (2013) for the same set of operating parameters and there was good agreement between that and the current result.

CONCLUSION

The parallel simulation of microparticles capture by an assemblage of ferromagnetic wires in axial magnetic filter was examined. A particle equation of motion taking into account the

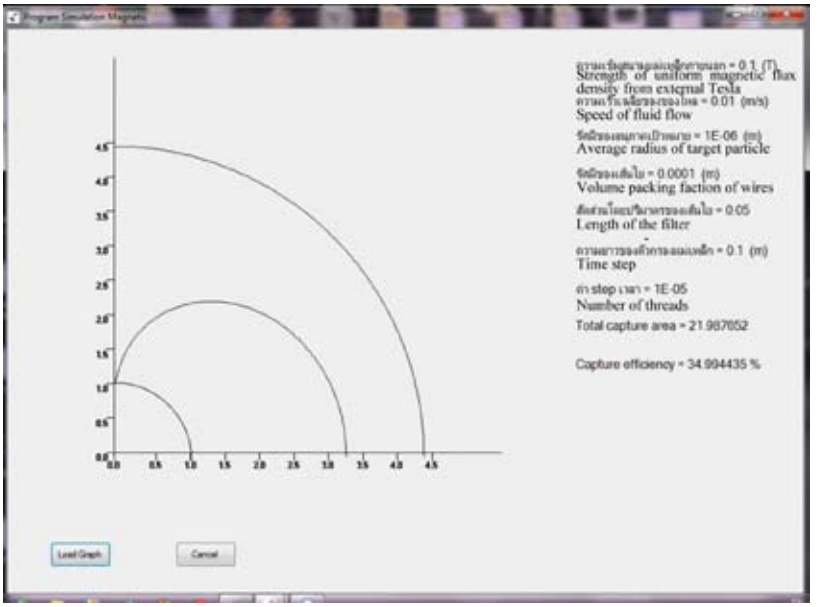

Figure 9 Result window with a superimposed English translation for clarification in the figure.

influences from the magnetic and fluid drag forces was formulated and then solved numerically, using the 4th-order Runge-Kutta method, to trace the particle trajectory. A large number of possible trajectories was determined and analyzed to predict the filter efficiency. This work concentrated on speeding up the task of computing the large number of particle trajectories using parallel simulation to compute the simulation results. The programming platform was based on OpenMP. The computing tasks were distributed to threads which can compute each trajectory independently. The graphic user interface allowed the user to explore different parameters for the simulations and view the prediction of capture efficiency in real-time. The parallel simulation helped the user to obtain the predicted filter efficiency for a set of operating parameters with a speed up of up to 5.27 times.

ACKNOWLEDGEMENTS

This work was supported in part by the Silpakorn University Research and Development Institute.

LITERATURE CITED

Bhakdi, S. C., A. Ottinger, S. Somsri, P. Sratongno, P. Pannadaporn, P. Chimma, P. Malasit, K. Pattanapanyasat and H. PH. Neumann. 2010. Optimized high gradient magnetic separation for isolation of Plasmodium-infected red blood cells. **Malar. J.** 9: 38–46.

Chantrapornchai, C., S. Dainparprai and O. Wongtaweesap. 2012. On the computer simulation of microparticles capture in magnetic filters using OpenMP. **Int. J. Comput. Appl.** 51: 23–30.

Hackett, S., J. Hamzah, T.M.E. Davis and T.G. St Pierre. 2009. Magnetic susceptibility of iron in malaria-infected red blood cells. **Biochim. Biophys. Acta.** 1792: 93–99.

Han, K.-H. and A. B. Frazier. 2006. Paramagnetic capture mode magnetophoretic microseparator for high efficiency blood cell separations. **Lab. Chip.** 6: 265–273.

Happel, J. 1959. Viscous flow relative to arrays of cylinders. **AIChE J.** 5: 174–177.

Hiroshi, U., A. Kho, K. Kazuhiro, F. Mitsuho, F. Shuichiro and I. Atsushi. 2009. Design and test of filter of high gradient magnetic separation system for trapping immunoglobulin in serum. **IEEE Trans. Appl. Supercond.** 19: 2157–2161.

Hournkumnuard, K. and M. Natenapit. 2013. The capture of micro-particles by random cylindrical wires in axial magnetic filters. **Sep. Sci. Technol.** 48: 2234–2242.

Inglis, D.W., R. Riehn, J. C. Sturm and R. H. Austin. 2006. Microfluidic high gradient magnetic cell separation. **J. Appl. Phys.** 99: 1–3.

Jung, J. and K.-H. Han. 2008. Lateral-driven continuous magnetophoretic separation of blood cells. **Appl. Phys. Lett.** 93: 223–902.

Melville, D., F. Paul and S. Roath. 1975. High gradient magnetic separation of red cells from whole blood. **IEEE Trans. Magn.** 11: 1701–1704.

Merino-Martos, A., J. de Vicente, L. Cruz-Pizarro, I. de Vicente. 2011. Setting up high gradient magnetic separation for combating eutrophication of inland waters. **J. Hazard. Mater.** 186: 2068–2074.

Natenapit, M. and W. Sanglek. 1999. Capture radius of magnetic particles in random cylindrical matrices in high gradient magnetic separation. **J. Appl. Phys.** 85: 600–603.

Norina, S.-B. and A. N. Shalygin 2014. Measurements of Magnetic Moments of Bio-Microparticles. **Biochem. Biophys.** 2: 1–6.

Philipp, S., H.H. Oberg, O. Janssen, M. Leippe and C. Gelhaus. 2012. Isolation of erythrocytes infected with viable early stages of *Plasmodium falciparum* by flow cytometry. **Cytometry.** 81: 1048–1054.

Ribaut, C., A. Berry, S. Chevalley, K. Reybier, I. Morlais, D. Parzy, F. Nepveu, F. Benoit-Vical and A. Valentin. 2008. Concentration and purification by magnetic separation of the erythrocytic stages of all human Plamodium species. **Malar. J.** 7: 45–49.